International Journal of Geosynthetics and Ground Engineering (2021) 7:15
https://doi.org/10.1007/s40891-021-00261-2

TECHNICAL NOTE

End Bearing Capacity Factor for Annular Foundations Embedded in Clay Considering the Effect of the Adhesion Factor

Suraparb Keawsawasvong[1] · **Van Qui Lai**[2,3]

Received: 27 October 2020 / Accepted: 5 February 2021 / Published online: 3 March 2021

Abstract

New limit analysis solutions for the end bearing capacity of annular foundations in clay with linearly increasing shear strength are presented in the paper. The strength profile of clay corresponds to a typical case of a normally consolidated clay in deep water, where the strength at the ground surface is defined as zero and increases linearly with the depth. The annular foundation has internal and external radii and is embedded in clay, where the adhesion factor representing the strength at the soil-structure interface is also taken into account. Using the lower and upper bound finite element limit analysis, the end bearing capacity factor of this problem can be obtained based on three considered dimensionless parameters, which are the ratio between the internal radius and the external radius, the embedded depth ratio, and the adhesion factor. The collapse mechanisms of annular foundations in clay are also examined and discussed in the paper to portray the effects of the radius ratio, the depth ratio, and the adhesion factor.

Keywords Bearing capacity · Annular foundation · Adhesion factor · Linearly increasing strength · Limit analysis

Introduction

A ring foundation is commonly used to support axisymmetric structures such as silos, water towers, storage tanks, transmission towers, chimneys, and bridge piers. The use of this kind of foundation can reduce the amount of constructing material which results in a more economical design. To investigate the bearing capacity of ring foundations, Saha [1] and Saran et al. [2] performed experiments for determining the bearing capacity of ring foundations resting on a sand layer. Using the method of characteristics, Kumar and Ghosh [3] presented the plastic solutions for the bearing capacity factor of ring foundations with smooth and rough soil-structure interfaces. The finite difference method was also employed by Zhao and Wang [4] to derive the solutions of the vertical bearing capacity for ring footings on cohesionless soil. Benmebarek et al. [5] and Remadna et al. [6] used the FLAC code to numerically investigate the bearing capacity factors of smooth and rough ring foundations on soils by considering the effects of associated and non-associated flow rules. The bearing capacity factors including N_c, N_q, and N_γ for ring foundations were proposed by Kumar and Chakraborty [7] using the finite element limit analysis and Keshavarz and Kumar [8] using the method of characteristics. Tang and Phoon [9] employed the finite element limit analysis to examine the influence of the stress level effect on the bearing capacity of ring foundations on dense sand. For the cases of ring foundations on layered soils, some researchers have presented the bearing capacity of ring foundations resting on two-layered soils for the cases of two-layered clays [10], sand overlying clay [11], and weak sand overlying dense sand [12, 13]. In addition, various researchers have also investigated the bearing capacity of a ring or circular foundation resting on the surface of reinforced soil (e.g., [14–18]).

All aforementioned works were the studies regarding the bearing capacity of the ring foundation resting on the surface of soils in which the effect of embedded depth was not

✉ Suraparb Keawsawasvong
suraparb@hotmail.com

1 Department of Civil Engineering, Thammasat School of Engineering, Thammasat University, Pathumthani, Thailand

2 Faculty of Civil Engineering, Ho Chi Minh City University of Technology (HCMUT), 268 Ly Thuong Kiet Street, District 10, Ho Chi Minh City, Vietnam

3 Vietnam National University Ho Chi Minh City (VNU-HCM), Linh Trung Ward, Thu Duc District, Ho Chi Minh City, Vietnam

taken into account. An annular foundation with an embedded depth is more suitable and economical and can carry the load transferred from axisymmetric structures such as offshore structures. Benmebarek et al. [19] and Lee et al. [20] have proposed the solutions for the annular foundation embedded in clay with constant shear strength and linearly increasing shear strength with depth, respectively. However, the existing solutions by Benmebarek et al. [19] and Lee et al. [20] considered only the cases of annular foundations with the rough interface condition. The effects of the ratio between the internal radius and the external radius, the embedded depth ratio, and the adhesion factor at the soil-foundation interface have never been considered together in the literature.

Problem Definition

This paper aims to present new bearing capacity solutions for annular foundations embedded in clay with linearly increasing shear strength as shown in Fig. 1. The annular foundation has internal radius r_i and external radius r_o and is embedded in clay with the depth L. The shear strength of clay increases linearly with the depth from the ground surface, as given by Eq. (1).

$$s_u = s_{u0} + \rho z, \tag{1}$$

where s_{u0} is the shear strength at the ground surface,
ρ is the linear strength gradient,
z is the depth measured from the ground surface.

This study considers only the case of $s_{u0}=0$, which corresponds to a normally consolidated clay in a very deep offshore area. As a result, the strength of clay at any depth can be expressed as $s_u=\rho z$. Note that this assumption of increasing shear strength has been considered by several works in the past for solving the capacity of offshore foundations (e.g., [21–25]). It should be noted that several real cases elaborated that the shear strength represented by SPT, Vs, and CPT could increase with depth (e.g., [35, 36]).

It is well recognized that the magnitude of the bearing capacity of foundations is commonly affected by the roughness at the soil-foundation interface, which is defined by the adhesion factor (α). The definition of this factor is the ratio between the undrained shear strength at the soil-foundation interface and that of the surrounding soil, which can be expressed in Eq. (2).

$$\alpha = \frac{s_{ui}}{s_u}, \tag{2}$$

where s_{ui} is the undrained shear strength at the soil-foundation interface, and s_u is the undrained shear strength of the surrounding soil. The complete range of the adhesion factor varies from 0 (fully smooth interface) to 1 (fully rough interface). Note that the existing solutions in the work by Lee et al. [20] are limited to the case of the rough interface ($\alpha=1$). This study considers the complete cases of $\alpha=0$, 0.25, 0.5, 0.75, and 1, which is the novel finding of this paper. It should be also noted that several previous works have proofed that the variation of the adhesion factor has a significant impact on the magnitude of the foundation capacity (e.g., [22–29]).

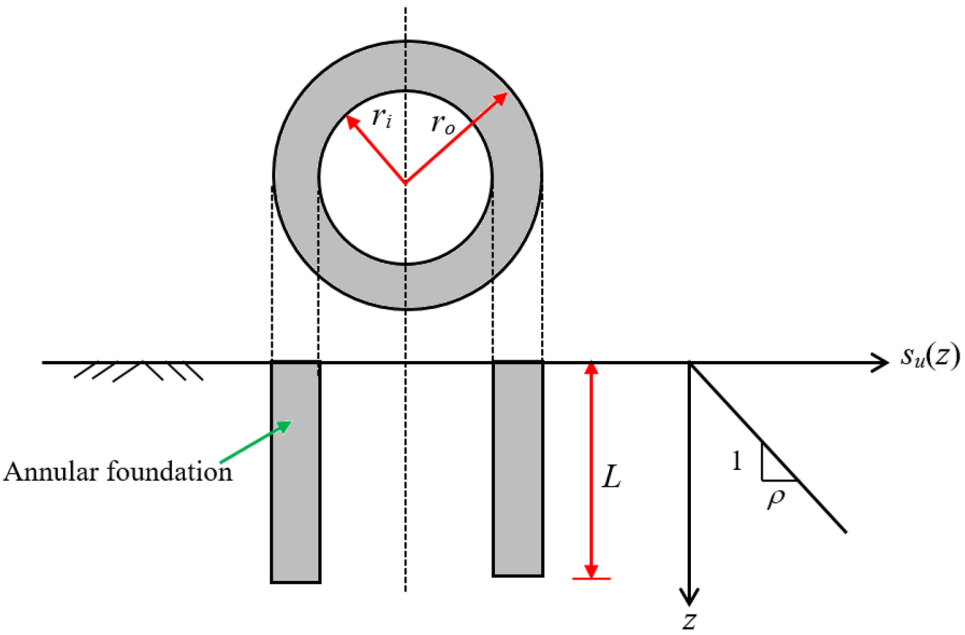

Fig. 1 Problem geometry of a rigid annular foundation embedded in clay

In this work, the embedded annular foundation has an internal radius r_i and an external radius r_o and is subjected to the vertical uniform pressure q applied at the top surface of the annular foundation. By integrating the vertical uniform pressure, the total vertical force Q can be represented as the relation to internal and external radii as shown in Eq. (3):

$$Q = \pi(r_o^2 - r_i^2)q. \tag{3}$$

The end bearing capacity factor of the annular foundation is defined as $q/\rho L$. To avoid the effect of the skin friction or the shaft resistances of the annular foundation on the end bearing capacity factor, the condition of the smooth interface ($\alpha = 0$) is strictly imposed at the surrounding surfaces inside and outside of the annular foundation while all roughness conditions (e.g., $\alpha = 0$, 0.25, 0.5, 0.75 and 1) are defined only at the base of the foundation. It can be summarized that three dimensionless input parameters have significant influences on the end bearing capacity factor of the annular foundation as shown in Eq. (4):

$$\frac{q}{\rho L} \propto f\left(\frac{r_i}{r_o}, \frac{L}{r_o}, \alpha\right), \tag{4}$$

where r_i/r_o is the radius ratio, L/r_o is the depth ratio, α is the adhesion factor applied at the base of the annular foundation.

It should be noted that only the N_c factor (in this study defined as $q/\rho L$) indicating the effect of the cohesion of clay is considered in the present study, where the N_q and N_γ factors indicating the effects of the overburden pressure and the unit weight of soil are not taken into account. As a result, all numerical models in the present study are set to be the cases of weightless soils and there is no surcharge applied at the ground surface of soils.

The finite element limit analysis (FELA) is carried out to derive the new solutions of the end bearing capacity factor of this problem. The FELA utilizes the optimization techniques in conjunction with finite element discretization techniques to provide the upper bound (UB) or lower bound (LB) solutions of the end bearing factor of the annular foundation. The formulations of UB and LB FELA are based on the plastic bound theorems cooperating with governing kinematic or equilibrium equations, respectively [30–32]. Using FELA, the end bearing factor can be accurately acquired by bracketing the results obtained from UB and LB methods in which the impacts of the radius ratio r_i/r_o, the depth ratio L/r_o, and the adhesion factor at the base of the foundation α can be examined. Furthermore, the collapsed mechanisms of annular foundations embedded in clay with undrained shear strength increasing linearly with depth are also illustrated, where the effect of the adhesion factor at the base of the foundation is also taken into account.

Numerical Methods

The LB and UB FELA [32] are employed to derive the end bearing capacity solutions of annular foundations embedded in clay with linear increasing undrained shear strength as shown in Fig. 1. To perform the numerical computation, the OptumG2 FELA software [33] is used to solve the solutions of this problem under axisymmetric conditions.

Note that the OptumG2 FELA software [33] has been recently used to study several bearing capacity problems (e.g., [11, 37–40]). Figure 2 depicts the simulation of an annular foundation embedded in clay modeled by OptumG2. Since the geometry of the problem is axisymmetric, only half of the model domain is used in the simulation, where the line of axial symmetry is set to be located at the left of the domain (see Fig. 2). The boundary conditions of the domain of this problem are described hereafter. The left and right boundaries of the domain are permitted to have only vertical movements whereas horizontal movements are not allowed. At the bottom boundary of the domain, it is set to be no movement in both horizontal and vertical directions. The top boundary of the domain is the free surface in which both horizontal and vertical movements are allowed to be taken place.

To model the annular foundation, rigid volume elements are carried out to simulate the annular foundation, where

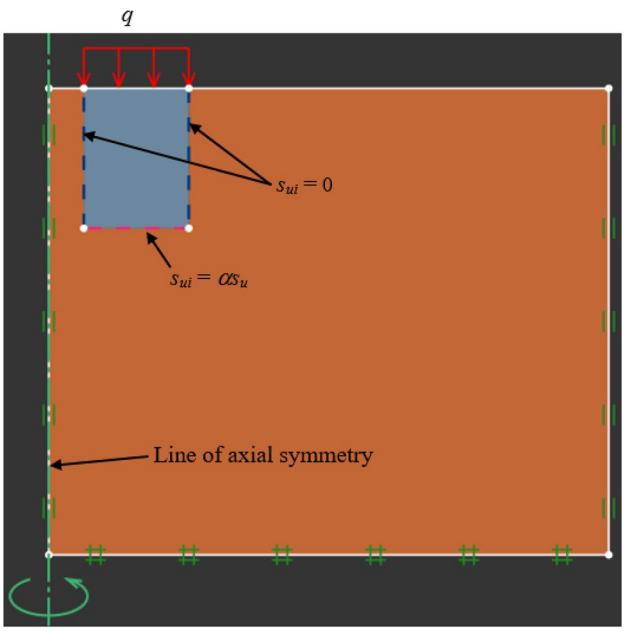

Fig. 2 A numerical model of a rigid annular foundation embedded in clay in OptumG2

the weight of all volume elements of the annular foundation is zero. Note that the annular foundation is perfectly rigid. At the top of the annular foundation, the vertical uniform pressure q is applied over the area from the inner radius to the outer radius of the foundation. The clay is also modeled using weightless volume elements, and has the strength at the ground surface being zero, and increasing linearly with depth (see Fig. 1). The failure criterion of clay is the Tresca failure criterion with an associated flow rule. Note that the reason for using weightless elements is to omit the effect of soil weight on the undrained end bearing capacity of this problem. Hence, the computed results from FELA in this study are in the scope of the stability problem under undrained conditions. At the left and right surfaces of the annular foundation, the smooth interface condition ($\alpha=0$) is applied at both sides of the inside and outside surfaces to avoid the effect of the skin friction or the shaft resistances (see Fig. 2). At the base of the annular foundation, the roughness conditions varying from $\alpha=0$ to $\alpha=1$ is set at the base (see Fig. 2). As a result, the end bearing capacity factors computed from FELA are purely affected by the adhesion factor defined at the base of the foundation.

To avoid the insufficient boundary effect, the sizes of the domains are chosen to be sufficiently large for all numerical models of annular foundation problems. Thus, the intersection of the plastic shear zone to the right and bottom boundaries of the domain is not permitted to occur. However, the intersection of the plastic shear zone to the left boundary (at the line of axial symmetry) and the top boundary (free surface) can take place. To increase the accuracy of the computed numerical results from UB and LB FELA, the automatic mesh adaptivity, which is a feature in OptumG2, is employed in the computation. This feature can improve the accuracy of the computed UB and LB bearing capacity solutions. During the process of the automatic mesh adaptivity, the number of elements will extremely increase in the zone that has high plastic shearing strain from the first step to the final step of mesh adaptivity iterations. More information regarding the automatic mesh adaptivity in OptumG2 can be found in Ciria et al. [34]. In this study, five adaptive steps are chosen, where the setup of the first adaptivity iteration is the use of 5000 elements while that of the fifth adaptivity iteration (or final adaptivity iteration) is approximately 10,000 elements.

Numerical Results and Discussion

The results of the end bearing capacity factor are first verified with the existing solutions by Lee et al. [20] for the cases of the rough interface condition ($\alpha=1$) defined at the base of foundations. Table 1 shows a comparison between the present FELA results and those FEM results from Lee et al. [20] for the cases of ring foundations resting on the surface of clays ($L/r_o=0$) by varying the shear strength at the ground surface s_{u0}. In Table 1, the normalized strength gradient is defined as $\rho r_o/s_{u0}$ and the end bearing capacity factor is defined as q/s_{u0}. The average (Avg) solutions shown in Table 1 are the average values from the UB and LB FELA solutions. It can be found from Table 1 that the FEM results by Lee et al. [20] are slightly larger than the Avg FELA solutions about 0.2–0.9%.

Table 1 A comparison of obtained q/s_{u0} values with the existing solutions by Lee et al. [20] for the cases of $L/r_o=0$

$\rho r_o/s_{u0}$	r_i/r_o	Lee et al. [20]	Present study		
		q/s_{u0} (FEM)	q/s_{u0} (LB)	q/s_{u0} (UB)	q/s_{u0} (avg)
0	0.00	6.08	6.02	6.06	6.04
0	0.25	5.92	5.87	5.92	5.90
0	0.50	5.61	5.55	5.60	5.58
1	0.00	7.64	7.60	7.64	7.62
1	0.25	7.03	6.95	7.01	6.98
1	0.50	6.40	6.33	6.39	6.36
5	0.00	11.42	11.32	11.38	11.35
5	0.25	9.68	9.58	9.66	9.62
5	0.50	8.44	8.32	8.41	8.37
15	0.00	18.03	17.91	18.01	17.96
15	0.25	14.14	13.97	14.11	14.04
15	0.50	11.76	11.60	11.73	11.67

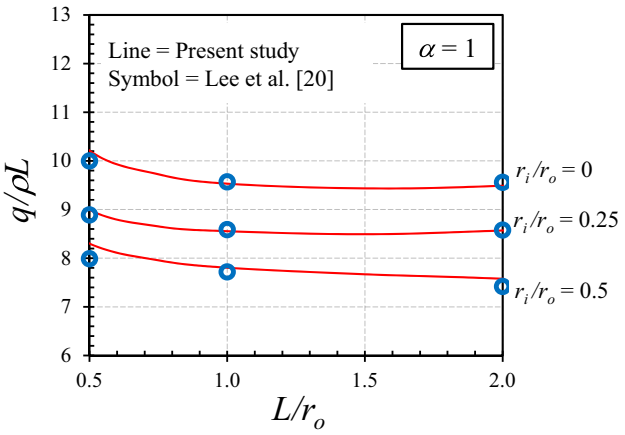

Fig. 3 Comparison of end bearing capacity factors for rough annular foundations embedded in clay ($\alpha=1$)

Figure 3 presents a comparison of the present study and the existing solutions by Lee et al. [20] for the cases of annular foundations embedded in clay. In Fig. 3, the existing solutions by Lee et al. [20] for the cases of $\rho r_o/s_{u0}=15$ are employed for the verification. Note that all solutions presented in Fig. 3 and hereafter in this paper are the average (Avg) solutions of the end bearing capacity factor defined

as $q/\rho L$. It can be seen from Fig. 3 that the present solutions agree very well with those of Lee et al. [20]. It should be noted that the results by Lee et al. [20] are limited to the cases of the rough interface condition, which are not the practical value of the roughness at the soil-foundation interface. The value of the inherent adhesion factor is in between rough ($\alpha = 1$) to smooth ($\alpha = 0$) conditions.

Table 2 shows the percent of the difference between the UB and LB solutions of the end bearing capacity factor defined as $q/\rho L$. The %Diff in Table 2 can be calculated as shown in Eq. (5):

$$\%\text{Diff} = \frac{\left[\left(\frac{q}{\rho L_{(\text{UB})}}\right) - \left(\frac{q}{\rho L_{(\text{LB})}}\right)\right] \times 100\%}{\left[\left(\frac{q}{\rho L_{(\text{UB})}}\right) + \left(\frac{q}{\rho L_{(\text{LB})}}\right)\right]/2}. \quad (5)$$

It can be found from Table 2 that the %Diff is less than 1.3% for all cases expressed in Table 2.

The end bearing capacity factors of annular foundations embedded in clay with linearly increasing strength by considering the adhesion factor are presented in Fig. 4a–e for the different values of $\alpha = 1$, 0.75, 0.5, 0.25, and 0, respectively. These figures show the relationship between the end bearing capacity factors $q/\rho L$ and the depth ratio L/r_o. The contour lines in Fig. 4 represent the values of r_i/r_o varying from 0, 0.25, and 0.5, respectively. It can be seen from Fig. 4 that the relationship between $q/\rho L$ and L/r_o is highly non-linear. When the value of r_i/r_o is equal to 0.5, the variation of $q/\rho L$ decreases as L/r_o increases. However, for the cases of $r_i/r_o = 0$ and 0.25, the value of $q/\rho L$ reduces when the value of L/r_o increases, and reaches the lowest point at L/r_o is about 1 or 1.5. After the lowest point, the value of $q/\rho L$ turns to increase when L/r_o increases. It is also found from Fig. 4 that an increase in r_i/r_o results in a decrease in $q/\rho L$. The effect of the adhesion factor on the end bearing capacity factor is demonstrated in Fig. 5a–d for the cases of $L/r_o = 0.25$, 0.5, 2, and 3, respectively. The relationship between $q/\rho L$ and α is non-linear. The influence of α is prominent when $L/r_o = 0.25$ and 0.5 (shallow foundations) as can be seen in Fig. 5a, b. The impact of α on the end bearing capacity factor becomes less when the depth of a foundation is large (see Fig. 5c, d).

Table 2 The percent of the difference between the UB and LB solutions

L/r_o	α	r_i/r_o	$q/\rho L_{(\text{LB})}$	$q/\rho L_{(\text{UB})}$	%Diff (%)
0.5	0.5	0.00	9.77	9.83	0.61
0.5	0.5	0.25	8.72	8.81	1.02
0.5	0.5	0.50	8.21	8.30	1.10
0.5	1	0.00	10.18	10.24	0.64
0.5	1	0.25	8.94	9.05	1.27
0.5	1	0.50	8.25	8.35	1.29
2	0.5	0.00	9.41	9.48	0.70
2	0.5	0.25	8.48	8.59	1.20
2	0.5	0.50	7.28	7.33	0.76
2	1	0.00	9.45	9.53	0.76
2	1	0.25	8.52	8.62	1.26
2	1	0.50	7.53	7.62	1.11

The impacts of L/r_o, r_i/r_o, and α on the collapsed mechanisms of annular foundations embedded in clay with linearly increasing strength are demonstrated hereafter. Figure 6 shows the influence of L/r_o on the final adaptive meshes of annular foundations embedded in clay for the cases of constant values of $\alpha = 1$ and $r_i/r_o = 0.5$. Note that many elements extremely increase in the zones that contain very high plastic shear strains due to the feature of the automatic mesh adaptivity by OptumG2 [33, 34]. This can imply the correctness of the numerical results from the FELA simulations certainly reaches the very accurate values of the end bearing capacity factor of annular foundations embedded in clay. Figure 7 also presents the effect of L/r_o on the incremental shear strain contours of annular foundations for the cases of $\alpha = 1$ and $r_i/r_o = 0.5$. It can be seen from Figs. 6 and 7 that the final adaptive meshes and the incremental shear strain contours can be used to demonstrate the collapsed mechanisms of the annular foundation problem since the plastic shear zones take place at the same locations. From Figs. 6 and 7, the shape of the plastic shear zones is log-spiral that extends from the bases of annular foundations to the free surface of the clay. An increase in L/r_o results in a decrease in the size of the plastic shear zones. The deepness of the plastic shear zones for the cases of $L/r_o = 0.25$, 0.75, and 2 are approximately $1L$, $0.5L$, and $0.3L$, respectively. Figure 8 demonstrates the effect of r_i/r_o on the incremental shear strain contours of annular foundations for the cases of $\alpha = 1$ and $L/r_o = 0.75$. The case of $r_i/r_o = 0$ reveals only one log-spiral plastic shear zone extending from the right corner to the free surface. However, when $r_i/r_o > 0$ (e.g., $r_i/r_o = 0.25$ and 0.5), two log-spiral plastic shear zones extending from both left and right corners appear. In addition, the size of the plastic shear zone also depends on the magnitude of r_i/r_o, where an increase in r_i/r_o yields a decrease in the size of the plastic shear zone. Figure 9 presents the examples of the base pressure distributions (or normal pressures) below the footing bases of annular foundations for the cases of $\alpha = 1$ and $L/r_o = 0.75$. It is found that the base pressures are not uniform, where the shapes of the base pressures significantly depend on the values of r_i/r_o as shown in Fig. 9. The effect of α on the incremental shear strain contours of annular foundations embedded in clay is demonstrated in Fig. 10 for the cases of $r_i/r_o = 0.25$ and $L/r_o = 1$. It can be found that the size of the plastic shear zone for the foundation with the smooth interface condition ($\alpha = 0$) is smallest,

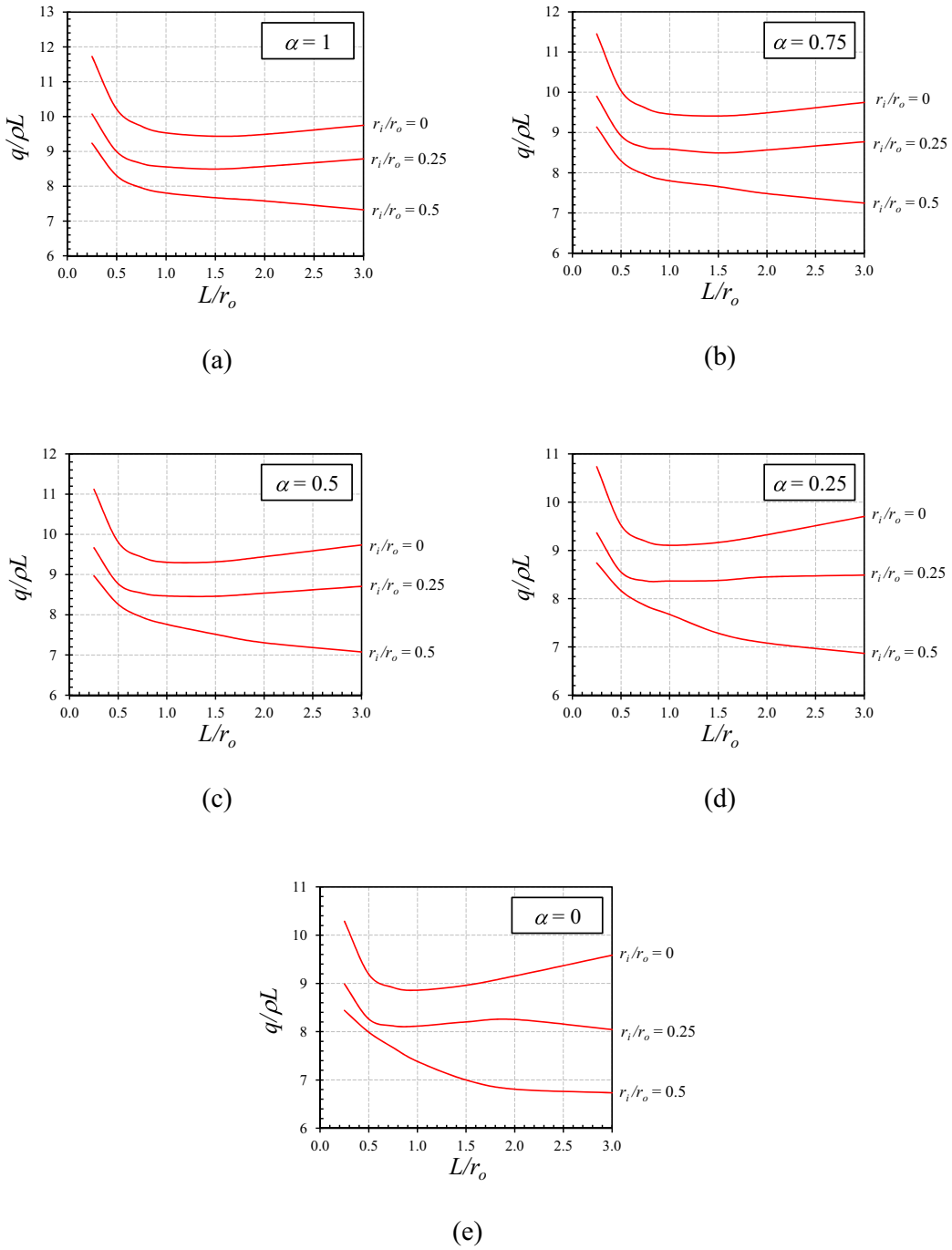

Fig. 4 End bearing capacity of annular foundations embedded in clay, where **a** $\alpha = 1$; **b** $\alpha = 0.75$; **c** $\alpha = 0.5$; and **d** $\alpha = 0.25$; and **e** $\alpha = 0$

and vertically expanded when the value of α increases. The biggest size of the plastic shear zone in Fig. 10 is the case with the rough interface condition ($\alpha = 1$).

Conclusions

In the paper, new plastic solutions for the end bearing capacity of annular foundations in clay with linearly increasing shear strength are presented, where the adhesion factor at the base of foundations are considered. Using the lower and upper bound finite element limit analysis with the automatic mesh adaptivity feature, the solutions

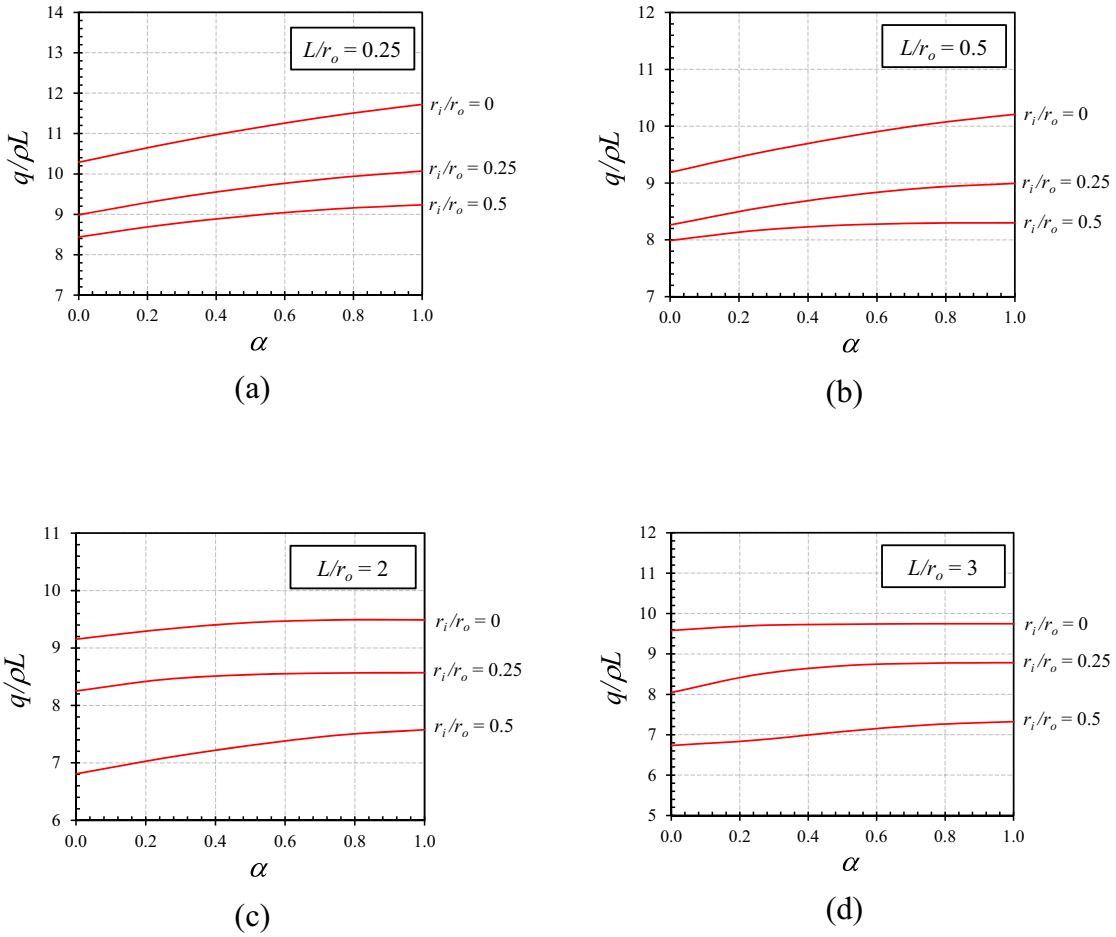

Fig. 5 End bearing capacity of annular foundations embedded in clay, where **a** $L/r_o = 0.25$; **b** $L/r_o = 0.5$; **c** $L/r_o = 2$; and **d** $L/r_o = 3$

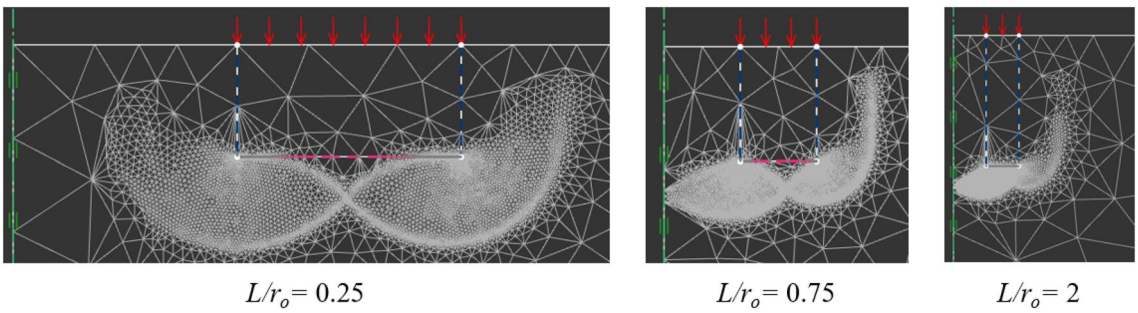

Fig. 6 Effect of L/r_o on the final adaptive meshes of annular foundations embedded in clay with $\alpha = 1$ and $r_i/r_o = 0.5$

of the end bearing capacity factor of annular foundations in clay can be obtained. The main results of the present study can be summarized as follows.

- In the verification, the present FELA solutions are larger than the existing FEM solutions by Lee et al. [20] about 0.2–0.9% for the cases of $L = 0$. For the cases of $L > 0$, the present FELA solutions are in good agreement with those from Lee et al. [20].
- The end bearing capacity factor is significantly influenced by three dimensionless parameters including the ratio between the internal radius and the external radius, the embedded depth ratio, and the adhesion factor.

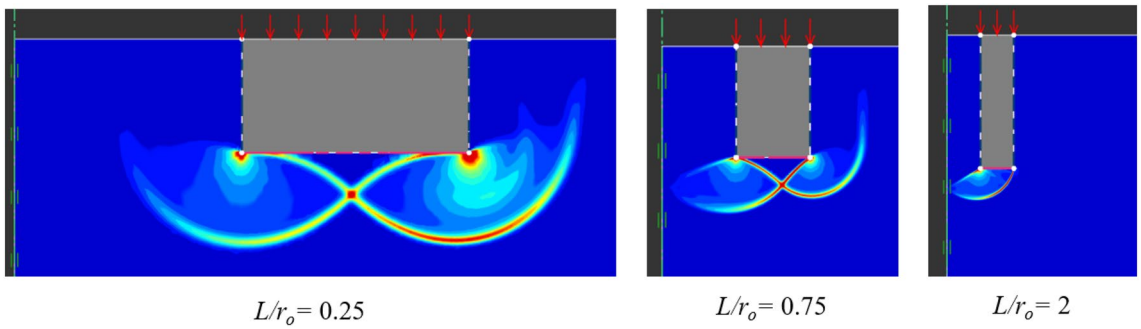

Fig. 7 Effect of L/r_o on the incremental shear strain contours of annular foundations embedded in clay with $\alpha = 1$ and $r_i/r_o = 0.5$

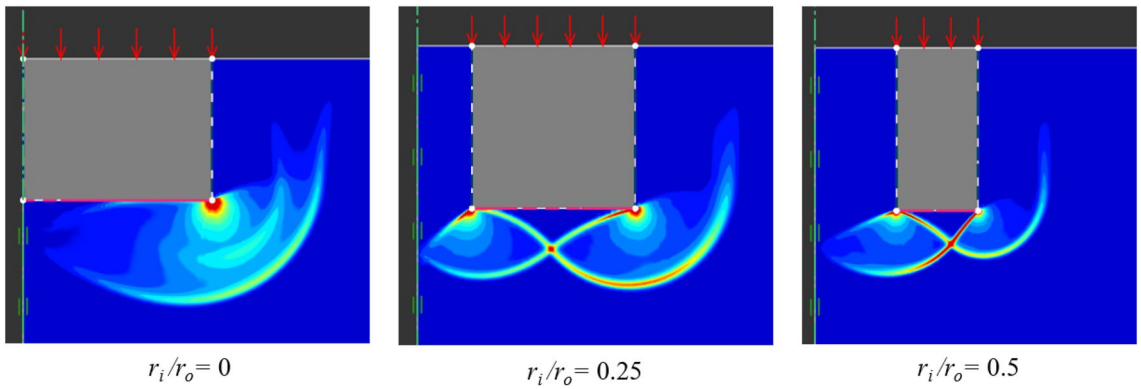

Fig. 8 Effect of r_i/r_o on the incremental shear strain contours of annular foundations embedded in clay with $\alpha = 1$ and $L/r_o = 0.75$

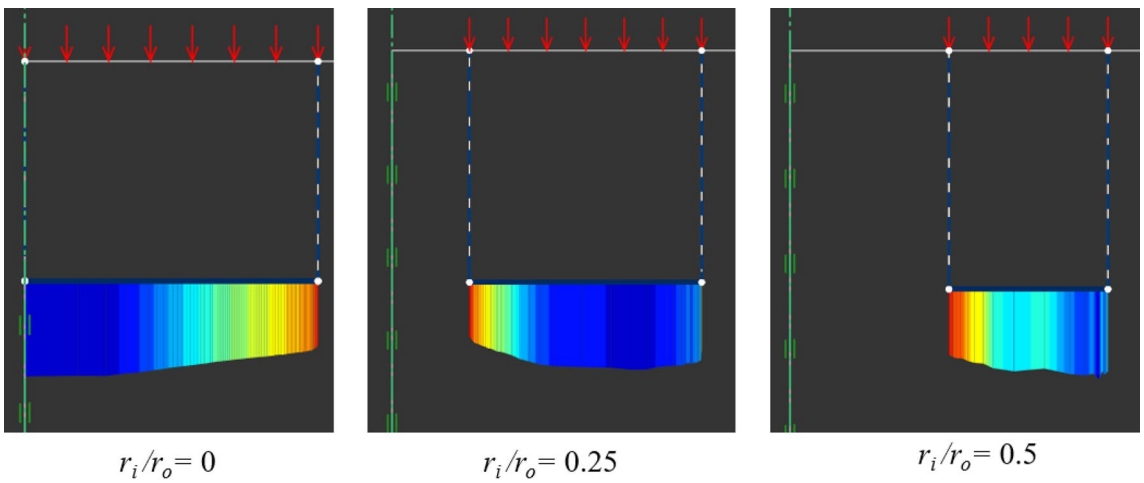

Fig. 9 Effect of r_i/r_o on the base pressure distributions below the footing bases of annular foundations embedded in clay with $\alpha = 1$ and $L/r_o = 0.75$

- For the collapse mechanisms of this problem, it is found that the size of the plastic shear zone becomes smaller when the depth of foundations becomes larger.
- The shapes of the plastic shear zones between the case of $r_i/r_o = 0$ and that of $r_i/r_o > 0$ are different, where one log-spiral shear zone appears in the cases of $r_i/r_o = 0$ whereas the case of $r_i/r_o > 0$ has two log-spiral shear zone taking

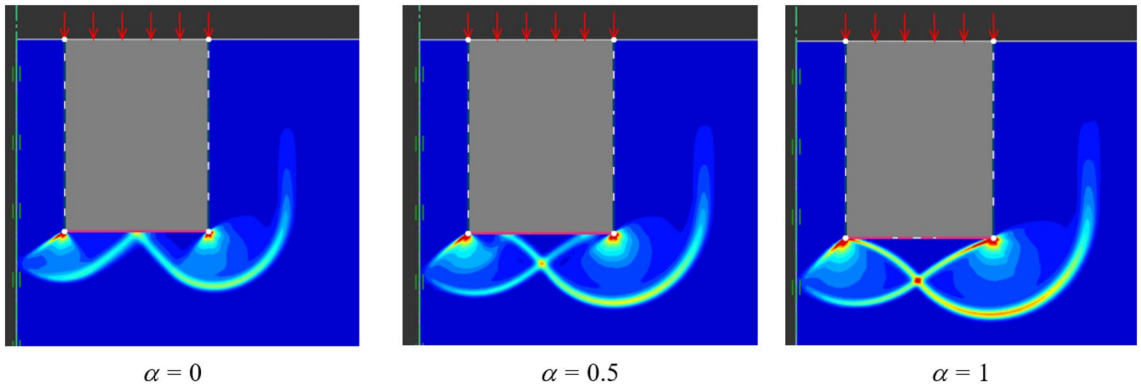

Fig. 10 Effect of α on the incremental shear strain contours of annular foundations embedded in clay with $r_i/r_o = 0.25$ and $L/r_o = 1$

place at the left and the right of the base of the annular foundation.

- For the effect of the adhesion factor at the base of foundations on the collapse mechanisms, the size of the plastic shear zone becomes bigger when the value of α becomes larger.

Author contributions SK acquired supervision, software, methodology and contributed to investigation and data curation, and writing—original draft. VQL provided resources and contributed to writing—review and editing.

Availability of data and material The data and materials in this paper are available.

Compliance with Ethical Standards

Conflict of interest The authors declare that they have no conflicts of interest to this work.

References

1. Saha, M.C. (1978) Ultimate bearing capacity of ring footings on sand. M.Eng. Thesis. UP, University of Roorkee, India.
2. Saran S, Bhandari NM, Al-Smadi MMA (2003) Analysis of eccentrically–obliquely loaded ring footings on sand. Indian Geotechnical Journal 33(4):422–446
3. Kumar J, Ghosh P (2005) Bearing capacity factor N. Can Geotech J 42:1474–1484
4. Zhao L, Wang JH (2008) Vertical bearing capacity for ring footings. Comput Geotech 35:292–304
5. Benmebarek S, Remadna MS, Benmebarek N, Belounar L (2012) Numerical evaluation of the bearing capacity factor of ring footings. Comput Geotech 44:132–138
6. Remadna MS, Benmebarek S, Benmebarek N (2017) Numerical evaluation of the bearing capacity factor N'c of circular and ring footings. Geomechanics and Geoengineering 12(1):1–13
7. Kumar J, Chakraborty M (2015) Bearing capacity factors for ring foundations. Journal of Geotechnical and Geoenvironmental Engineering 141:06015007
8. Keshavarz A, Kumar J (2017) Bearing capacity computation for a ring foundation using the stress characteristics method. Comput Geotech 89:33–42
9. Tang C, Phoon KK (2018) Prediction of bearing capacity of ring foundation on dense sand with regard to stress level effect". International Jornal of Geomechanics 18:04018154
10. Lee JK, Jeong S, Shang JQ (2016) Undrained bearing capacity of ring foundations on two-layered clays. Ocean Eng 119:47–57
11. Yang C, Zhu Z, Xiao Y (2020) Bearing capacity of ring foundations on sand overlying clay. Applied Sciences 10:4675
12. Das PP, Khatri VN, Dutta RK (2019) Bearing capacity of ring footing on weak sand layer overlying a dense sand deposit. Geomechanics and Geoengineering. https://doi.org/10.1080/17486025.2019.1664775
13. Khatri VN, Kumar J, Das PP (2020) Bearing capacity of ring footings placed on dense sand underlain by a loose sand layer. European Journal of Environmental and Civil Engineering. https://doi.org/10.1080/19648189.2020.1805643
14. Boushehrian JH, Hataf N (2003) Experimental and numerical investigation of the bearing capacity of model circular and ring footings on reinforced sand. Geotext Geomembr 21:241–256
15. Sharma V, Kumar A (2017) Strength and bearing capacity of ring footings resting on fibre-reinforced sand. International Journal of Geosynthetics and Ground Engineering 3:9
16. Benmebarek S, Remadna A, Benmebarek N (2018) Numerical modelling of stone column installation effects on performance of circular footing. International Journal of Geosynthetics and Ground Engineering 4:23
17. Biswas A, Ansari MA, Dash SK, Krishna AM (2015) Behavior of geogrid reinforced foundation systems supported on clay subgrades of different strengths. International Journal of Geosynthetics and Ground Engineering 1:20
18. Badakhshan, E., Noorzad, A. (2017) .A simplified method for prediction of ultimate bearing capacity of eccentrically loaded foundation on geogrid reinforced sand bed. *International Journal of Geosynthetics and Ground Engineering*, 3, 14.
19. Benmebarek S, Saifi I, Benmebarek N (2017) Undrained vertical bearing capacity factors for ring shallow footings. Geotech Geol Eng 35:1–10
20. Lee JK, Jeong S, Lee S (2016) Undrained bearing capacity factors for ring footings in heterogeneous soil. Comput Geotech 75:103–111

21. Ukritchon B, Keawsawasvong S (2017) Unsafe error in conventional shape factor for shallow circular foundations in normally consolidated clays. Journal of Geotechnical and Geoenvironmental Engineering 143(6):02817001
22. Keawsawasvong S, Ukritchon B (2016) Finite element limit analysis of pullout capacity of planar caissons in clay. Comput Geotech 75:12–17
23. Ukritchon B, Keawsawasvong S (2016) Undrained pullout capacity of cylindrical suction caissons by finite element limit analysis. Comput Geotech 80:301–311
24. Ukritchon B, Wongtoythong P, Keawsawasvong S (2018) New design equation for undrained pullout capacity of suction caissons considering combined effects of caisson aspect ratio, adhesion factor at interface, and linearly increasing strength. Appl Ocean Res 75:1–14
25. Ukritchon B, Yoang S, Keawsawasvong S (2018) Bearing capacity of shallow foundations in clay with linear increase in strength and adhesion factor. Mar Georesour Geotechnol 36(4):438–451
26. Keawsawasvong S, Ukritchon B (2016) Ultimate lateral capacity of two dimensional plane strain rectangular pile in clay. Geomechanics and Engineering 11(2):235–251
27. Keawsawasvong S, Ukritchon B (2017) Undrained lateral capacity of I-shaped concrete piles. Songklanakarin Journal of Science and Technology 39(6):751–758
28. Ukritchon B, Keawsawasvong S (2018) Undrained lateral capacity of rectangular piles under a general loading direction and full flow mechanism. KSCE Journal of Civil Engineering 22(7):2256–2265
29. Ukritchon B, Keawsawasvong S (2019) Design equations of uplift capacity of circular piles in sands. Appl Ocean Res 90:101844
30. Drucker DC, Prager W, Greenberg HJ (1952) Extended limit design theorems for continuous media. Q Appl Math 9:381–389
31. Chen WF (1975) Limit analysis and soil plasticity. Elsevier, Amsterdam
32. Sloan SW (2013) Geotechnical stability analysis Géotechnique 63(7):531–572
33. Krabbenhoft, K., Lyamin, A., Krabbenhoft, J. (2015) Optum computational engineering (OptumG2), Available on: www.optumce.com
34. Ciria H, Peraire J, Bonet J (2008) Mesh adaptive computation of upper and lower bounds in limit analysis. Int J Numer Methods Eng 75:899–944
35. Likitlersuang S, Plengsiri P, Mase LZ, Tanapalungkorn W (2020) Influence of spatial variability of ground on seismic response analysis: a case study of Bangkok subsoils. Bull Eng Geol Environ 79(1):39–51
36. Misliniyati R, Mase LZ, Irsyam M, Hendriawan H, Sahadewa A (2019) Seismic response validation of simulated soil models to vertical array record during a strong qarthquake. J Eng Technol Sci 51(6):772–790
37. Keawsawasvong S, Thongchom C, Likitlersuang S (2020) Bearing capacity of strip footing on Hoek-Brown rock mass subjected to eccentric and inclined loading. Transport Infrastruct Geotechnol. https://doi.org/10.1007/s40515-020-00133-8
38. Ebrahimi K, Khazaei J (2019) Investigation of bearing capacity and failure pattern in shell foundations by FELA method. Geotech Geol Eng 37:3523–3534
39. Wu G, Zhao M, Zhao H, Xiao Y (2020) Effect of eccentric load on the undrained bearing capacity of strip footings above voids. Int J Geomech 20(7):04020078
40. Li C, Zhou A, Jiang P (2020) Eccentric bearing capacity of embedded strip footings placed on slopes. Comput Geotech 119:103352